

HTC Determination on 3D Geometries from Transient Thermochromic Liquid Crystal Experiments

Joshua R. Ryley^{*}, Matthew McGilvray[†] and David Gillespie[‡]

University of Oxford, Oxford, United Kingdom, OX1 3PJ

A valuable new post-processing technique has been developed to enable the application of transient thermochromic liquid crystal experiments where lateral conduction is significant, and thus, cannot be treated as one-dimensional. This enables the measurement of spatially resolved heat transfer coefficient over geometrically complex surfaces, extending the current limitations of transient thermochromic liquid crystal experiments. The post-processing technique couples raw experimental transient thermochromic liquid crystal data and finite element analysis, in an iterative procedure, to generate the heat transfer coefficient distributions. In the current study, the experimental data comes from a stationary experiment of an engine realistic rib turbulated cooling passage. Spatially resolved maps of heat transfer coefficient have been determined over the surface of the ribs. The results are compared to conventionally processed experimental data which assumes one-dimensional semi-infinite conduction and also to results from steady state numerical simulations. Where the one-dimensional assumption is applicable, results are less than the experimental uncertainty ($< 6\%$) at the majority of locations. Typical one-dimensional based methods are unable to provide reliable spatial measurements over geometrically complex ribbed surfaces and to the authors best knowledge this is the first time distributions of heat transfer coefficient have been reported for engine representative rib geometry.

^{*}DPhil, Department of Engineering Sciences, Parks Rd Oxford, joshryley@gmail.com

[†]Associate Professor, Department of Engineering Sciences, Parks Rd Oxford, matthew.mcgilvray@eng.ox.ac.uk

[‡]Associate Professor, Department of Engineering Sciences, Parks Rd Oxford,

Nomenclature

Symbols

c_p	Specific heat capacity at constant pressure, [J/(kg.K)]
D_h	Hydraulic diameter, [m]
e	Rib height , [m]
g	Acceleration due to gravity, [m/s ²]
H	Passage height, [m]
h	Heat transfer coefficient, [W/(m ² .K)]
I	Normalised light intensity in the green wavelength range
k	Thermal conductivity, [W/(m.K)]
l	Characteristic length, [m]
Nu	Nusselt number, $\frac{h.l}{k}$
p	Rib pitch, [m]
q	Heat flux, [W/m ²]
r	Radius, [m]
Re	Reynolds number, $\frac{\rho.v.l}{\mu}$
T	Temperature, [K]
t	Time, [s]
v	Velocity, [m/s]
W	Passage width, [m]
z	Material normal direction, [m]

Subscripts

g	Gas
i	Initial
s	Surface

Greek

α Rib angle, [°]

β Heat flux parameter, Equation 2

μ Viscosity, [Pa.s]

ρ Density, [kg/m³]

ϕ Damping Factor

Abbreviations

AR Aspect Ratio, (W/H)

ERICKA Engine Realistic Internal Cooling Knowledge Applications

FEA Finite Element Analysis

HTC Heat Transfer Coefficient

THTAC Transient Heat Transfer Analysis Code

TLC Thermochromic Liquid Crystal

I. Introduction

Many convective heat transfer experiments lack high resolution detail over complex surfaces, as most conventional methods have inherent limitations due to assumptions required in post-processing temperature data. To ensure the total surface heat transfer data is recorded, many experimental techniques measure average heat transfer over a large region [1]. Conventional transient thermochromic liquid crystal (TLC) experiments measure heat transfer coefficient (HTC) distributions by assuming a one-dimensional semi-infinite behaviour when solving the Fourier heat equation. However, for cases of highly 3D geometries or substantial levels of lateral conduction, this assumption is invalidated and a suitable one-dimensional solution does not exist.

With recent improvements both in computational power and software capabilities, it has now become viable to solve the transient 3D conduction problem in Finite Element Analysis (FEA) codes. On high curvature surfaces, where intensity data must be used from transient TLC experiments, the data are noisy and non-monotonic making transformation to the temperature field

impossible without prior assumption. This makes direct application of an FEA solver to the experimental heat conduction problem extremely difficult. In this paper, a new technique is developed to combine experimental information taken from transient TLC experiments and transient FEA simulations. This builds and extends upon work performed by Colletti et al. [2] who developed a similar technique for steady-state Infra-Red experiments. It also moves past the 2D transient inverse heat transfer work of Sousa et al. [3] by inclusion of complex 3D geometries.

The current technique moves past previous work of Lin and Wang [4] which accounted for lateral conduction, though only on simple geometries such as a flat plate. Their method combined hue based signals from a single wide band crystal during a transient TLC experiment and a 3D transient heat transfer computation in an iterative scheme. The method described in the current paper combines green intensity signals from multiple narrow band TLC, which are inherently more defined, and commercial finite element analysis solvers. The use of a commercial solver, enables a greater variety of geometries to be investigated, and more advanced meshing strategies to be used. The technique is able to process data from conventional transient TLC experiments and resolve HTC on a variety of surfaces. The new technique developed has been validated over a range of geometries and heat flux conditions.

The technique developed is applicable for a wide range of possible applications where 2D and 3D conduction effects make accurately resolving heat transfer coefficient (HTC) a challenge. An example is around the corners of turbine blade tips [5] where lateral conduction has led to high uncertainties in these measurements. This technique could also be simplified and applied to transient IR experiments. In this research, the new technique has been applied to internal cooling passage experiments. Turbine blades use internal cooling passages which contain rib turbulators to promote heat transfer by disrupting near wall flow. The highest HTC occurs on the ribs. The ribs also have largest gradients in HTC providing a particularly challenging region for CFD codes to accurately resolve. Currently very little experimental information is available about the distribution of HTC over these surfaces.

Improvement to both the accuracy and distribution for internal cooling passage heat transfer predictions in the design stage can lead to a significant reduction in specific fuel consumption,

environmental emissions and increased blade life. Numerous experimental campaigns have measured the performance, as average values or neglecting the ribs, over a variety of internal cooling passage configurations [1] and data from these experiments have been used in validation of numerical codes prediction of HTC. This has led to higher accuracy and increased use of numerical tools (CFD) in the design stage. Many different methodologies are employed for validating CFD for internal cooling passages ([6–8]), with the majority of the methods comparing bulk heat transfer coefficient values. In doing so they fail to evaluate whether detailed features are captured and potentially lead to unsuitable designs being implemented. Therefore, it is essential that spatially resolved maps of heat transfer are available for validation.

In studies which produce spatially resolved maps of HTC, (e.g. [9,10]) ribs have generally been excluded from transient TLC experiments due to 3D conduction effects. Some authors present information for the average HTC over ribbed surface (e.g. [11]). However it is currently unclear how much of an effect that applying an average value has on the design process. Few examples of spatial maps of HTC reported over ribbed surfaces exist. One example is the work by Coletti et al. [12] who used two configurations of a heated surface for steady state TLC experiments in order to provide spatial maps of HTC on both the ribs and planar surfaces. In this work the ribs had a sharp rectangular profile with the passage ribbed on one surface with jets impinging on the ribs. As two separate experiments (and heat element configurations) were required this may impact the heat transfer around the base of the rib due to the additional conduction. A second study by Coletti et al. [2] using the same test geometry reported values over the surface of the ribs, collected in a single test using steady state Infra-red thermography combined with FEA to solve the conduction in the solid. Both of these studies provide useful information about the HTC over the rib, however the idealised geometry and the presence of the impingement jets means that data is unsuited for validating CFD in the typical internal cooling passages found in the mid section of the blade.

This paper details the methodology of the new iterative transient FEA procedure which is able to solve for maps of heat transfer coefficient over geometrically complex surfaces. The new technique has been applied to experiments previously performed on a section stationary internal cooling passage, containing engine realistic features, at the University of Oxford [11]. Results are

presented for a section of the passage in the form of spatially resolved maps of HTC, including over the ribs. Five Reynolds numbers are investigated between 18,000-105,000 for two different aspect ratio passages, 1:2 and 1:3. The results are compared to available conventionally processed experimental and numerical data.

II. Transient Liquid Crystal Technique

The transient TLC technique makes use of the properties of encapsulated thermochromic liquid crystal which undergo a change in their reflective wavelength (and hence a colour change is observed) in an optically active temperature band (typically 1°C) depending on the chemical make-up. Outside this band, they appear optically transparent. Surface temperature information is visually recorded throughout a test. Tests typically start with isothermal solid and fluid, and a sudden change in temperature is applied to the gas. For the experiments undertaken in this paper, a near step increase in gas temperature is delivered from a heater mesh at the start of the test.

Green intensity history is currently used at Oxford, as it was found to provide a strong signal to noise ratio over a narrow temperature band. As surface temperature alters, and corresponding change in TLC activity occurs, a peak in green intensity is observed. One variant of transient technique uses a mixture of multiple crystals in a single layer which provides more information about the surface temperature history over a greater proportion of the test, as well as making it easier to capture a wide range of HTCs in a single test. For the current experiments, a mixture of three 1 degree Celsius narrow band TLC (25, 30 and 35 degrees C) was used. A theoretical green intensity response for the TLC mixture is presented in Figure 1. This is for a HTC of 200 W/m².K and a step change in gas temperature from 20 degrees to 50 degrees assuming initially isothermal conditions and is short enough duration that it behaves as semi-infinite conduction. The three peaks can be clearly seen, showing peaks when the TLCs are activated.

For recent experiments undertaken in Oxford, PMMA is used for the substrate material (thermal product, $569 \pm 29 \frac{W}{m^2 s^{0.5} K}$). PMMA provides good optical access for internal geometries with thermal properties in the range required for the experiments. For internal geometries, a mixture of the encapsulated TLC, three in this case, and mixed with a binder to the surface ($\approx 30 \mu m$) is

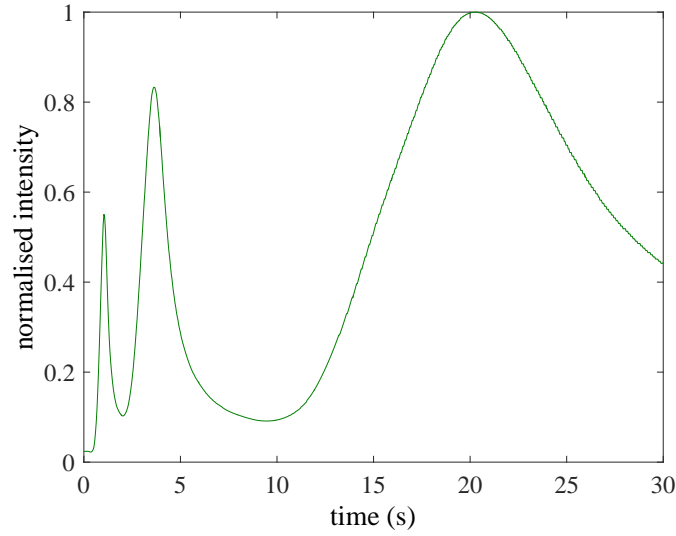


Figure 1. Green intensity response for a surface with three different liquid crystals applied. $HTC = 200 \text{ W/m}^2\cdot\text{K}$ and a step change in gas temperature from 20 to 50 degrees C.

then coated with black ink to reduce the transmitted light ($\approx 30 \mu\text{m}$). Previous work by Forsyth et al. [13] has shown that for this setup, the coatings cause insignificant difference of the experimental results.

Evaluation of the surface temperature response can be made through comparison of the times at which peaks in green intensity occur, or by analysis of the full green intensity profile. The latter method is more computationally expensive but is better conditioned provided the surface temperature response follows a known analytical form. The conventional method for processing transient TLC experiments is to solve the one-dimensional Fourier conduction equation, Equation 1, under semi-infinite initially isothermal conditions in the wall normal direction, to produce a surface temperature response for a specific HTC value. This surface temperature response is then converted, by means of a calibration, to an intensity history. An analytical solution for the HTC is determined by finding which HTC value provides a best match between the theoretical and experimental intensity histories. This evaluation can either be made as an iterative method, updating the HTC value until a required threshold is reached, or by comparing a discrete range of HTC values. More details of this TLC method can be found in [14].

$$\frac{\partial T}{\partial t} = -\frac{k}{\rho c_p} \frac{\partial^2 T}{\partial z^2} \quad (1)$$

The limitation of this method is that it assumes that conduction through the solid is purely 1D, making it unsuited for experiments with high levels of lateral conduction and complex geometries. Corrections exist for simple concave/convex geometries and lateral conduction [15–18]. However, these cannot extend to truly three dimensional surfaces.

III. Experimental Facility

A brief summary of the experimental facility and passage is described below, a more detailed description of the experiment and results can be found in the paper by Ryley et al. [11]. Figure 2 presents the stationary internal cooling rig, which includes a single pass of a rib turbulated passage. The experiment measures spatially resolved HTC values by using the transient TLC method. The rig is operated in suction mode, with the outlet plenum connected to a vacuum line, containing a gate valve to set the mass flow rate (measured with an orifice plate on the intake). A flow straightener and baffle plate are located before and after the test section respectively in order to promote flow uniformity through the passage. The heater mesh (50×50 mm), which is used to supply a difference in gas to wall temperature transiently, is situated 400 mm upstream of the contoured section to the internal cooling passage.

The internal cooling passage test section consists of a rectangular duct with corner fillets (radius of width/4) with rib turbulators on opposing walls and two smooth side walls, and is approximately five times engine scale. The passage width is 18.66 mm and the length of the passage is 432 mm. Two aspect ratios (width:height) of 1:2 and 1:3 were investigated by varying the height of the smooth walls, with rib blockage (e/D_h) of 6.9% and 6.2% and a hydraulic diameter of 26.1 and 29.0 mm respectively (calculated neglecting ribs). Ribs in the passage are: at an angle (α) of 45° to the streamwise direction; have a spacing (P/e) of 10; are filleted in all three directions (radius of filleting is $e/2$); are centred and span half the width of the passage; and are staggered by half the pitch.

Mirrors are placed above and below the test section at an angle of 45° , and allow the main camera to capture three of the surfaces during a single test. A second camera images a short section of the downstream ribbed wall to capture high spatial resolution data (~ 0.9 mm per pixel).

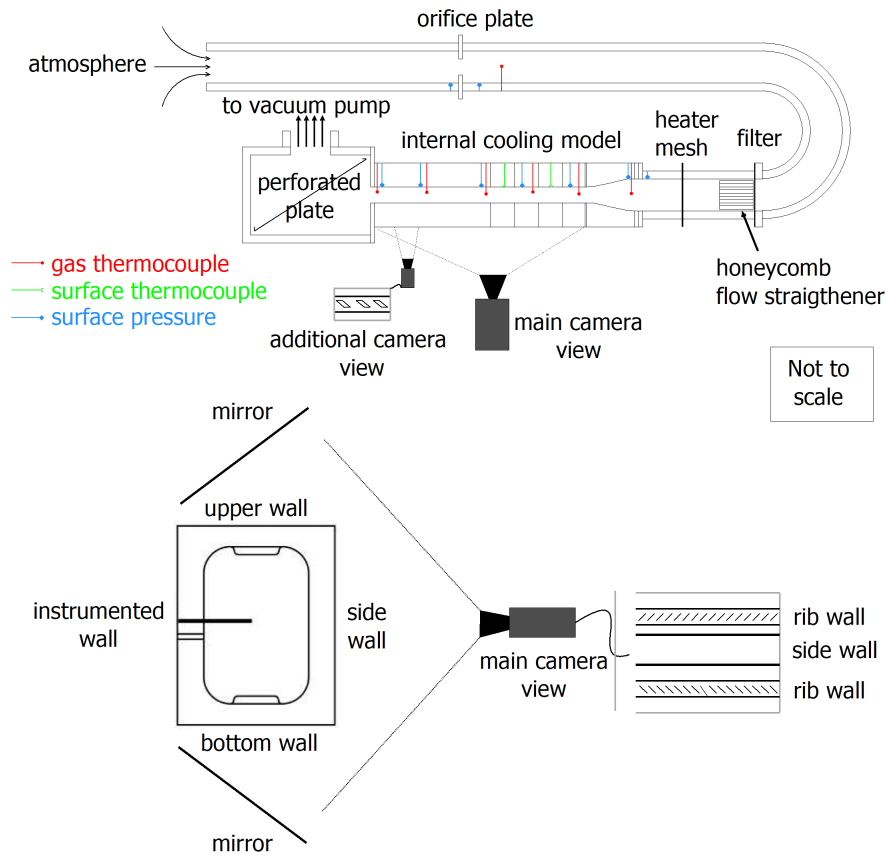


Figure 2. Schematic of experimental setup of flow path, instrumentation and camera view.

Data from this camera will be used in the work presented here. Five K-type gas thermocouple measurements were taken along the centreline.

The test section is constructed from PMMA, which has a thermal product $569 \pm 29 \frac{W}{m^2 s^{0.5} K}$ [19]. It is a good thermal insulator and provides optical access. The test duration used in the processing of the data was limited to 30 s, which is well below the time taken for the thermal pulse to reach the external surface and void the semi-infinite assumption [20]. The internal surface of the test section is coated with a mixture of a binder and three narrow band TLC (1°C activation, nominally 25, 30, and 35°C). A black ink backing is applied to provide better contrast.

The experimental HTC values are determined based on a linear interpolation of the centreline gas temperature measurements to each streamwise location. HTC values are evaluated at every pixel location using an in house code Transient Heat Transfer Analysis Code (THTAC) [21] which models the gas temperature as a series of ramps [14]. This is used for regions where the one-dimensional conduction is valid or as an initial estimate of values for the iterative FEA approach.

The analytical solution which provides a best fit is evaluated by finding which solution produces a minimum residual sum of squares difference between the experimental and theoretical green intensity histories.

To allow a hybrid rib technique to calculate the average values of HTC over the ribs [22], several of the PMMA ribs were replaced with brass inserts. This technique uses a lumped heat capacity model with temperature measured at the PMMA interface, as the inserts have a low Biot number. The brass inserts were backed with the same TLC mixture used on the passage walls to measure temperature and affixed to the PMMA with the binder. The rounded rectangular profile of the internal cooling passage requires a correction factor to be applied at the radial corners. The correction factor of Buttsworth and Jones [15] has been applied in these regions.

Calibration of all TLC was performed using a slowly rising gas temperature to maximise the accuracy, and made in-situ to remove distortion effects caused by lighting. The experimental uncertainty for the HTC values are from 6-18% depending on location [11]. Separate calibrations were performed for the PMMA surfaces and hybrid ribs.

IV. FEA geometry and settings

The region considered in this paper is one rib pitch in length (18 mm) as seen in Figure 3. The model extends to 45° on the passage fillet. This ensures good quality green intensity information is available over the full surface. A model of the test section is generated in COMSOL and the boundary conditions applied are shown in Figure 4. The minimum model depth normal to the top surface is 10 mm, which corresponds to a maximum test duration of 53 s according to the Schultz and Jones' [20] one-dimensional assumption criteria, and is less than the physical model depth used in the experiments. The FEA simulation is conducted for a test duration of 30 s equivalent to the experiment.

In simulating the transient experiments the material properties, density ($\rho = 1180 \text{ kg.m}^{-3}$), specific heat capacity ($c_p = 1444.1 \text{ J.kg}^{-1}.\text{K}^{-1}$) and thermal conductivity ($k = 0.19 \text{ W.m}^{-1}.\text{K}^{-1}$). This results in thermal product of $569 \text{ W.m}^{-2}.\text{s}^{-0.5}.\text{K}^{-1}$. The COMSOL model is meshed using an unstructured free tetrahedral mesh, with 871,511 elements. The mesh is restricted on the top

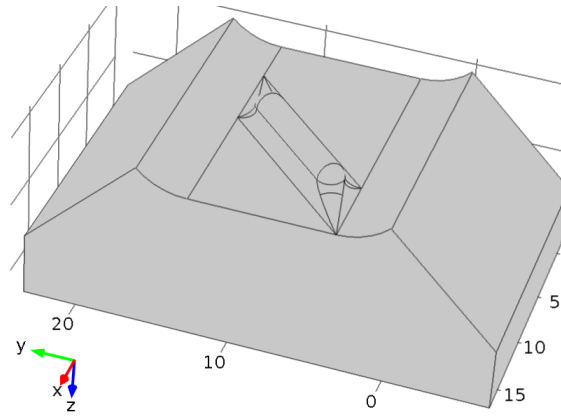


Figure 3. CAD model showing the experimental test section modelled in the iterative transient FEA.

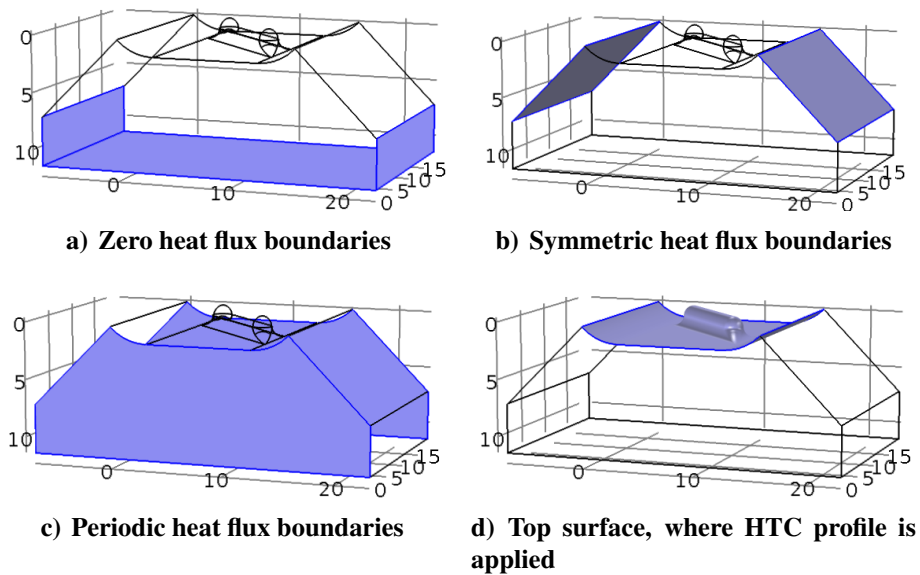


Figure 4. Heat flux boundary conditions applied to the FEA model.

(ribbed) surface, which corresponds to the image captured by the camera. This surface has a minimum element size of 0.0835mm, maximum element size of 0.25mm. COMSOL mesh settings were applied to specify the number of cells along curved surfaces and the growth rate of the cells in planar regions proximate to curved surfaces. These were namely a resolution of curvature of 0.1, and a growth rate of 1.15. The surface elements had 17,791 nodes which were used to import and export data via the MATLAB-COMSOL interface. The same mesh has been used for all cases investigated. Increasing the mesh density by 31% did not significantly affect the results (0.4% average difference).

V. Iterative Transient FEA Procedure

The conventional transient TLC technique is applicable for planar surfaces with low lateral conduction (i.e. dominated by wall normal conduction [16]) and, when a correction factor is applied, curved surfaces. However, this technique is not valid for more complex geometry where the one-dimensional assumption does not hold, such as a rib turbulator which is to be investigated here. A transient finite element analysis (FEA) has been chosen to solve the temperature field in both space and time around a rib turbulator where the one-dimensional Fourier equation is no longer valid. By coupling experimental green intensity data to a finite element model predicting temperature in the corresponding geometry, it is possible to generate a solution for the HTC, even under complex geometrical conditions. In order to achieve this, an iterative technique is required. The process is diagrammatically represented in Figure 5.

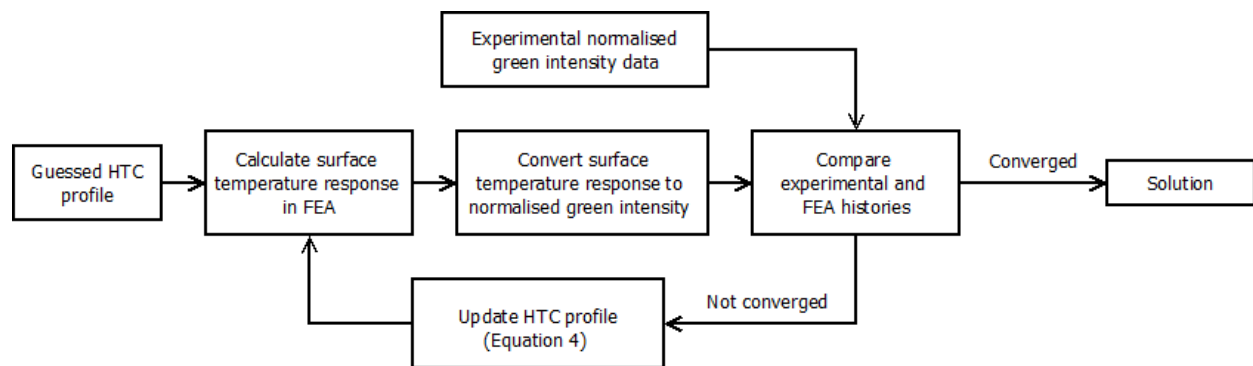


Figure 5. Schematic of the iterative process to determine the Heat Transfer Coefficient profile.

An initial guess of the heat transfer coefficient profile over the test geometry is applied to a finite element model. The numerical model is solved under the same boundary conditions as the experimental test. The surface temperature history from the FEA is then compared to the experimental surface temperature history (in the form of TLC activation). Based on the differences between the two surface temperature histories a new solution for the heat transfer coefficient profile is generated and fed back into the finite element model. This process is repeated until the two solutions converge to within a defined threshold at every spatial location.

For this research the transient finite element analysis is performed by the program COM-

SOL [23], calling upon the LiveLink tool via MATLAB [24]; this enables it to be called in an automated loop with updated variables, making it suited to this work.

A model of the test section is generated and meshed in COMSOL, and relevant mesh node locations exported. MATLAB is then used to generate the HTC profile at every location which is then passed back to the COMSOL environment every time the script is called. In the same manner the gas temperature history can be fed into COMSOL as a time dependent variable for the transient test. This value is not altered at each iteration and is constant throughout the test section.

When the simulation is completed the data is exported to be read by MATLAB. MATLAB is then used to compare the solution provided by COMSOL to the reference data and provide an updated HTC profile, which can then be fed back into COMSOL. This process is repeated for a fixed number of iterations.

In this research, experimental reference data are green intensity histories at every pixel location and theoretical data are surface temperature histories from the finite element model at mesh node locations on the corresponding model surface. This is then converted to a green intensity history, using the TLC calibration from the experiment. To solve for HTC the differences between the two sets of intensity histories are evaluated, an updated HTC map is generated, and the process repeated.

The updated HTC is generated by comparing the difference in time at which peaks in TLC intensity occur in both intensity histories (experimental and FEA simulations). Considering initially a green intensity history with only one crystal activation, the updated HTC value is generating using Equation 4. With multiple crystals this procedure can be repeated for all peaks in green intensity and an average updated HTC produced. By using multiple crystals the temperature history the solution more information on the surface temperature history is provided meaning a more accurate solution of HTC is likely to be produced.

Equation 4 has been derived from the case of one-dimensional conduction. Theta is defined by Equation 2 for a step change in gas temperature. For a surface temperature event (which corresponds to a peak in intensity) there is a fixed value of θ_1 for a given β_1 , i.e. θ is dependent on β only. β (Equation 2) is dependent on $h\sqrt{t}$ and $\sqrt{\rho ck}$ only, with $\sqrt{\rho ck}$ assumed as a constant. Under

the conditions of a perfect step it is possible to directly solve for an unknown HTC value given data concerning a pair of matched temperature events (θ and hence β) with one solution (theoretical) generated for a known HTC value using Equation 3.

Equation 4 uses this theory to generate an updated HTC profile based on the difference in TLC events, but with an additional variable, ϕ , which operates as a damping term ($0 < \phi \leq 1$). Under experimental conditions the change in gas temperature is not a perfect step and the potential for 3D conduction effects means that an iterative process is required to accurately evaluate the HTC for a given surface temperature response.

$$\theta = \frac{T_s - T_i}{T_g - T_i} = 1 - e^{\beta^2} \operatorname{erfc}(\beta), \quad \beta = \frac{h\sqrt{t}}{\sqrt{\rho ck}} \quad (2)$$

$$h_1 = h_2 \left(\frac{\sqrt{t_{peak\ 1}}}{\sqrt{t_{peak\ 2}}} \right) \quad (3)$$

$$h_{FEA\ new} = \phi \cdot h_{FEA} \left(\frac{\sqrt{t_{peak\ FEA}}}{\sqrt{t_{peak\ exp}}} \right) + h_{FEA} (1 - \phi) \quad (4)$$

It is noted that real gas temperature histories, especially as distance from the heater mesh increases, are rarely equivalent to a step change. A step change in gas temperature represents the most severe transition that can occur, and therefore a small change in the HTC value would correspond to a large change in time for a peak in green intensity (compared to a slower rise in gas temperature). This means that when updating for a new HTC value with realistic experimental gas temperature histories the equation is naturally damped, even when $\phi = 1$.

A. Use of experimental input data

The iterative transient FEA procedure has been applied to a section of the experimental facility, containing a single rib pitch. The experimental data are taken from the high resolution camera, situated in the downstream third of the experimental test section where the flow is more developed. The video is cropped around the central rib, located between 343-361 mm on the suction surface.

Every surface node location is assigned a corresponding pixel history based on a nearest evaluation. The experimental reference data, in the form of peak times, is extracted at every node.

Unlike the solutions generated based on the one-dimensional Fourier equation, each data point can impact its neighbours. To prevent this, data are rejected based on crystal inactivity, signal noise and viewing angle $> 70^\circ$. Finally, any outliers are rejected. At each location multiple peak times, up to a maximum of three can be present.

For the nodes located on the top of the rib, defined as locations above the point of inflection, the updated HTC value at every location is determined by the difference in time between the final peak which occurs in both the experimental and simulated results. This is due to the difficulty in reliably obtaining the earlier peaks, caused by high heat flux and noise. For the remaining surface nodes, the iterative technique calculates the updated HTC value based on the differences in time for all pairs of experimental and numerical peaks. The mean value is then taken as the updated value. This method is comparable to the best fitting method, based on the lowest residual sum of squares, used in the transient TLC processing and prevents the results being skewed towards one peak's information.

The iterative technique generates an HTC value for every location based on peak times. However, data on the peak times may not be available at every location, either through view obstruction or data rejection. At these locations a NaN value is assigned initially. Interpolation and/or extrapolation are used based on the neighbouring values to replace the NaN values with an HTC. This provides COMSOL with a 'best guess' to calculate the next series of temperature histories at each location.

At each node location smoothing is applied by taking an average of the data points and its nearest neighbours. Testing of the impact of the smoothing function on the iterative technique demonstrated little influence on the majority of points.

B. Technique validation

The FEA solutions of surface temperature history and the iterative process has been validated against a series of exact solutions for a range of geometries, HTC profiles and driving gas temperature histories typically observed in the experiments. A summary is given below:

- Iterative method shown to produce converged solutions to within 1% for a flat plate for five

HTC values between 50-1250 W/(m².K) for six gas temperature histories.

- FEA solutions for transient temperature rise matched the analytical solutions for flat plate and concave surfaces well within 0.1 K by 0.2 s into the simulation.
- Iterative technique has been applied to a series of complex HTC profiles, for a range of geometries. These included a target HTC profile consisting of an abruptly alternating pattern of two HTC values. The greatest difference observed (for a pattern of 200 - 1000 W/(m².K)) had a maximum local error of 15% and an average error of 0.9%.
- Ideal simulations conducted on the experimental ribbed geometry used similarly complex HTC profiles which resulted in a maximum localised error of 10.1% and an average error of 0.5%.

An example validation is presented in Figure 6. First, transient FEA is used to calculate the surface temperature history at each location for the target HTC distribution shown in Figure 6a). This is converted to a normalised green intensity history using the experimental calibration. This provides the pseudo experimental data. Secondly, the iterative transient FEA procedure is undertaken using the pseudo experimental data and a uniform HTC of 500 W/m².K as an initial guess. As shown in Figure 6b), the iterative method produces a result with an average error in HTC within 1% to the target HTC distribution, with some extremely localised discrepancies as high as 10% observed at the abrupt changes in HTC.

In summary, the validation work demonstrated that the modelling in FEA and iterative procedure is able to handle complex HTC profiles, with large gradients, and produce accurate solutions which are consistent when the initial guess is altered. This indicates that the technique is robust and suitable for a wide range of applications, without modification or further instrumentation in the test rig.

VI. Results

Simulations have been run for two the two aspect ratio passages experimentally investigated at five different Reynolds numbers. For all test cases 15 iterations were performed. This takes approx-

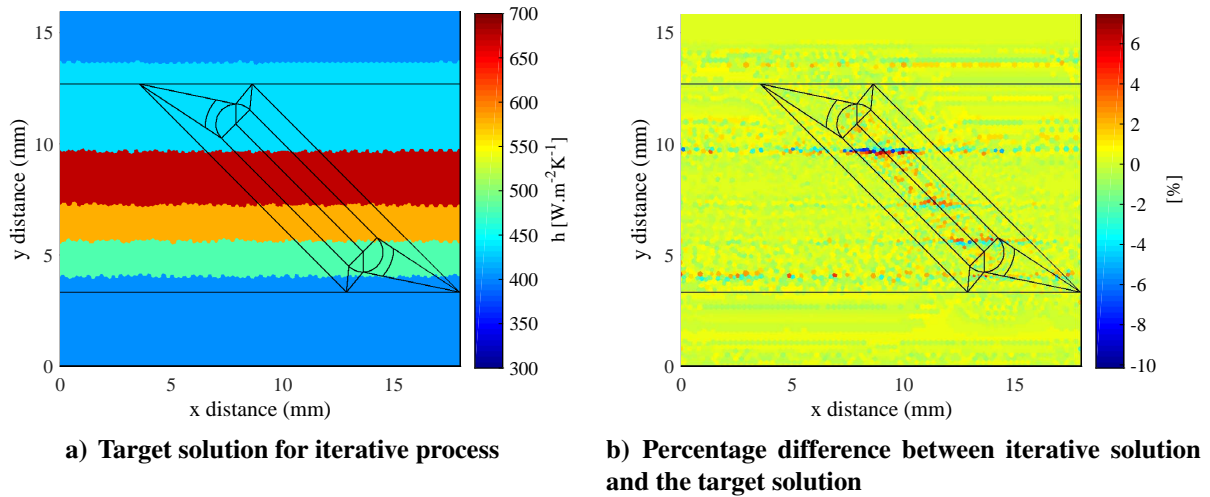


Figure 6. Robustness testing of the iterative transient FEA procedure.

imately 36 hrs to run on a dual core, 3.4 GHz PC with 8 GB of RAM. This number was chosen from preliminary work where solutions always converged. For all cases investigated the maximum change in HTC at any individual location during the last two iterations fell to within 2.5%. The iterative transient FEA procedure has been repeated for different values of initial HTC, which produced a solution within 1% at every location. In addition, excellent agreement was found in repeated experiments at matched experimental conditions.

An example of the results produced by the transient iterative FEA process is shown in Figure 7a), with the corresponding 1D solutions in Figure 7b). These results are for an aspect ratio passage of 1:2 and a Reynolds number of 60,506. Results are presented on a logarithmic scale for clarity. Data from the one-dimensional analysis show good agreement to the FEA solution in the flat part of the passage and on the major fillet which has a radial correction applied. Typically for the majority of locations this agreement is within 10% for all cases investigated. However, it can be seen there are extremely large discrepancies on the rib itself (outlined in a black box) where the one-dimensional assumption is invalid. Also, THTAC has struggled to even provide a reasonable match in the high HTC locations.

Figure 8 presents three typical fits between the experimental green intensity histories and those generated by FEA for the HTC profile in Figure 7 at the labelled locations. The two data sets show good agreement at all locations, indicating that the HTC profile is correct. Figures 8b) and

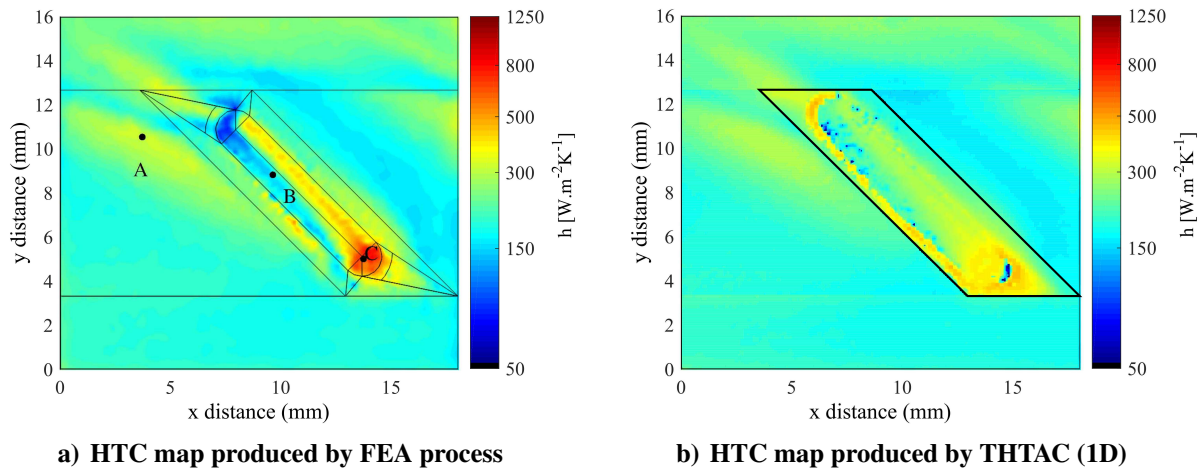


Figure 7. Maps of HTC for the 1:2 aspect ratio, at a $Re = 60,500$ on a logarithmic scale. Points A-C are locations where the green intensity history is examined

c) demonstrate a stronger agreement with the final peak than the earlier peaks, and this is due to the iterative technique used over the rib. If an incorrect HTC profile had been assigned an inferior agreement between all the peaks would be observed.

The calculated HTC profile over the surface of the rib reveals a complex structure with large variations. The highest values are seen on the upstream tip of the rib (marked by position C in the bottom right of Figure 8a) where the bulk flow direction is from right to left). In contrast the lowest values of HTC are located on the opposite end of the rib (downstream tip, top left corner). The maximum values are approximately 10 times greater than the minimum. This indicates that there is significant HTC gradients are set up over rib.

The experimental HTC profile derived using 1D solution, and application of the radial correction factor, provide a target solution for the transient iterative FEA profile. Where there is no experimental data, extrapolated values are used to allow comparison to the FEA results. Typical agreement between the semi-empirical and FEA results lies within 10% for the majority of locations. For all cases the average difference between comparable locations is under 6%. The method used to provide the best fit result between the analytical solutions and the experimental data in the transient TLC processing method is different to the method used in FEA method, and therefore small differences are expected. An example of the percentage difference between the two solutions for the HTC maps shown in Figure 9. In this figure the majority of the results lie within 5%, on

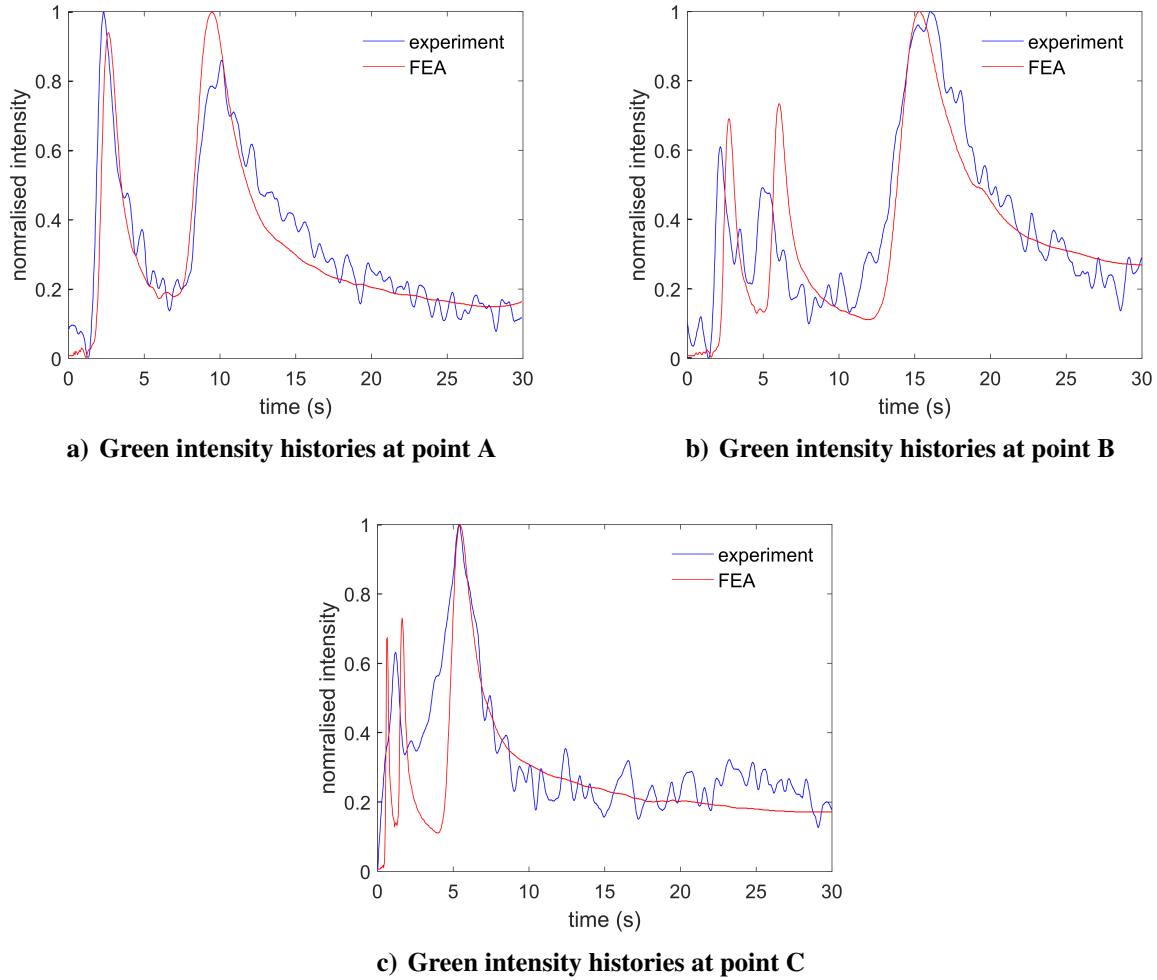


Figure 8. Green intensity histories at the points identified in Figure 7.

both the planar and radial walls. This provides good validation that the iterative transient FEA technique is correctly providing a solution for the HTC profile. The region where the rib is located is removed.

Along the streamwise edges there is an observed increase in the difference between the results from the one-dimensional method and the FEA simulation. This is an artefact of the periodic boundary condition applied along the two boundaries at these locations. The experimental data are not truly periodic and this leads to heat flux through the boundaries and a locally incorrect solution in these regions. This was investigated by applying a symmetric boundary condition along these edges, resulting in a closer agreement. These local errors however have little impact on the HTC profile derived over the rib, and therefore are not significant when considering the aim of this work.

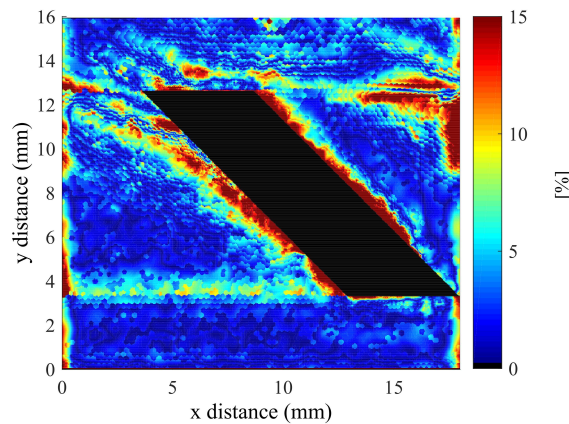


Figure 9. Absolute percentage difference between HTC maps generated by FEA and THTAC and AR=1:2, Re = 60,500

Increased difference between the two solutions observed around the edges of the rib are speculated to be caused by continued lateral conduction from proximity to 3D geometry.

Impact of Reynolds number and aspect ratio

Figure 10 present the full surface maps of the HTC provided by the transient iterative FEA method for both aspect ratio passages at the lowest, middle and highest Reynolds numbers tested. The maps have been cropped to show the results on and immediately around the rib. As expected the HTC values on the rib for both aspect ratios tend to increase with increasing Reynolds number. The overall pattern of HTC remains the same, however steeper gradients of HTC are seen for the lower Reynolds number cases.

Comparison of the HTC profiles between the two aspect ratio passages show that the same general trend is observed. High HTC values are seen on the upstream (right hand) side of the rib with low values on the downstream (left hand) side, this effect is more pronounced at lower Reynolds numbers. Differences do exist, such as in the 1:3 aspect ratio passage where a region of increased HTC is observed on the upstream side rib corner (located approximately at $x=9$, $y=11$ mm). In addition on the downstream side of the rib in the same location the very low HTC values observed in the 1:2 aspect ratio passage are significantly increased (for the 1:3 case). This shift in heat transfer distribution may be linked to the strengthening of the secondary flow as evidenced previously, see [11].

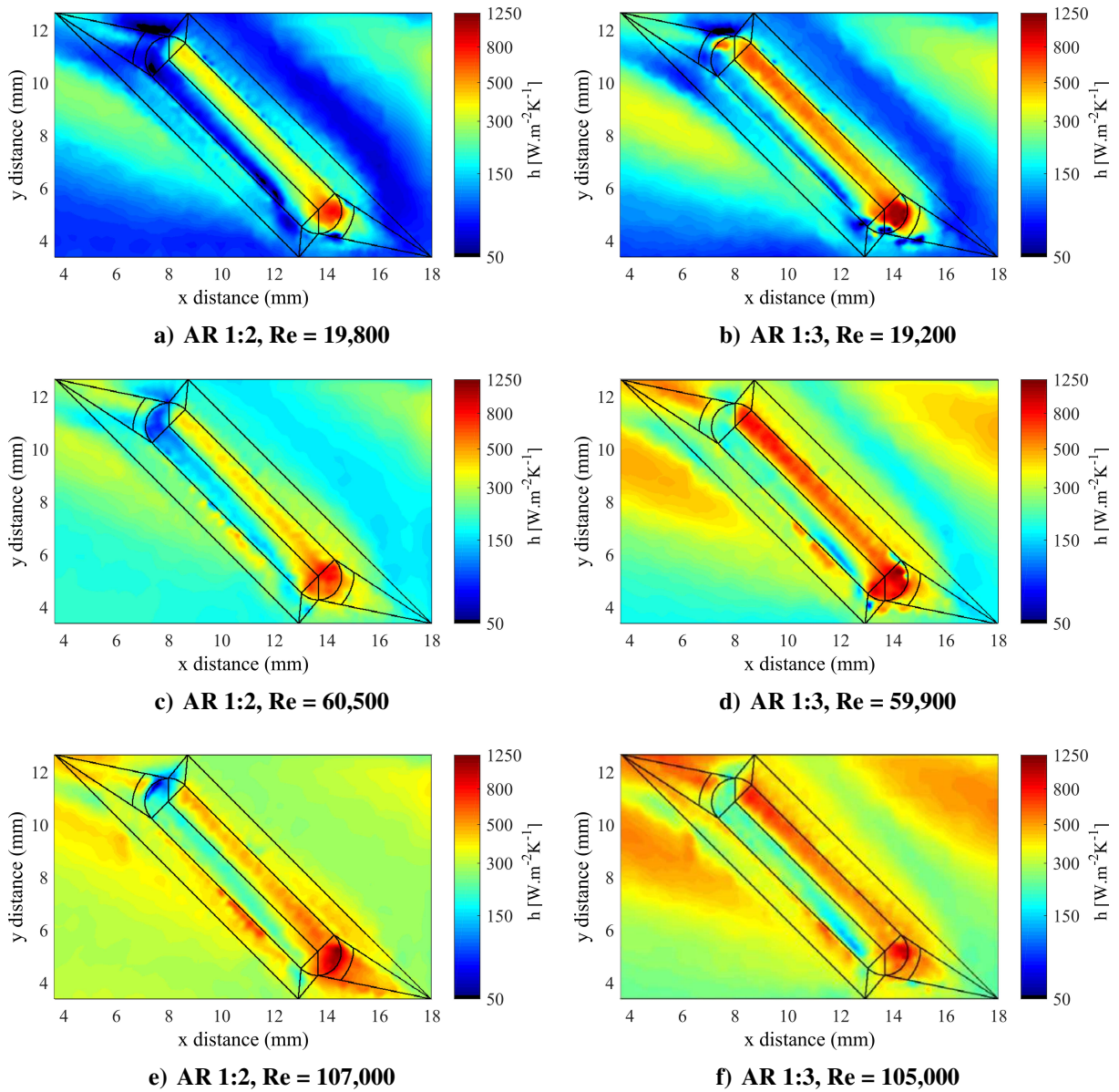


Figure 10. HTC profiles for different aspect ratios and Reynolds number

Further comparisons can be made to of average measurements of HTC over the ribs. The full experimental passage contains brass rib inserts on the the ribbed wall opposing the surface currently investigated. This allowed a ‘hybrid rib’ technique to be employed yielding average HTC measurements. For the simulations the average value on the rib is calculated using an area weighted average HTC value. Both sets of HTC values are based on the projected area. Figure 11 plots the result of the simulated average values of HTC and two sets of experimentally measured average HTC values. The first is provided by the hybrid technique at approximately the same

streamwise location on the opposite ribbed wall. For the planar surfaces the pattern and magnitude of the HTC distribution does not agree completely. This may be expected as the staggered ribbed geometry induces a secondary flow field that is not entirely symmetrical. An alternative data set from the hybrid technique has been also been plotted for comparison. This second data set is again provided from the opposite ribbed wall, not at the same streamwise position, but rather chosen by matching the magnitude of the downstream reattachment region on the floor of the passage. It can be observed from the full experimental data maps that there is strong coupling between the magnitude of the HTC in the reattachment region and the average value over the rib [11]. The data shows better agreement to this latter map.

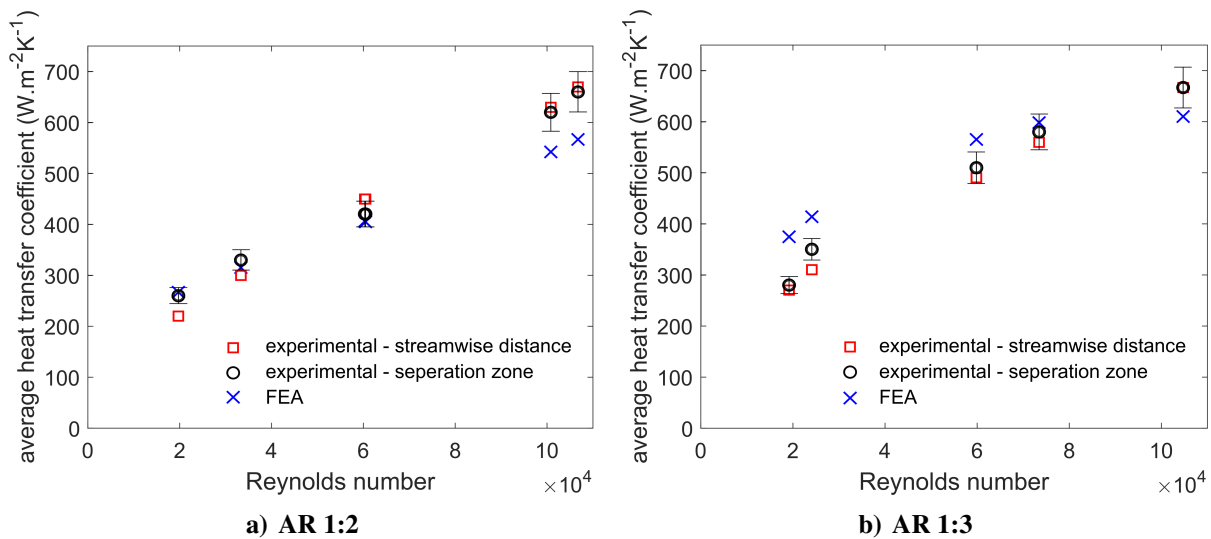


Figure 11. Average HTC over the rib (based on projected area) vs. Reynolds number

The majority of the FEA values lie within 15% of the average HTC value based on the matched reattachment regions, with the one exception of the lowest Reynolds number conditions at the aspect ratio 1:3. It is believed that this higher discrepancy is due to high heat flux conditions in the experiment on the surface of the rib, making the temperature events unreliable. The work performed on the 1:2 aspect ratio passage shows closer agreement to the hybrid rib values at lower Reynolds numbers. Increased differences are also observed at the higher Reynolds number cases (>90,000), these are subject to further investigation.

Comparison to CFD results

Complimentary CFD has been run for the whole experimental test section at a Reynolds number of approximately $Re = 60,000$. Several two equation turbulence models have been investigated, and in general the best agreement between the experimental results (on the planar surfaces) was found using a realizable $k-\epsilon$ turbulence model. This model is used for comparison, and details can be found in McGilvray et al. [25]. The CFD results are extracted from the highest density mesh simulations developed in a larger study which used ANSYS FLUENT 13.1 [26]. For all cases, Y^+ is below 0.5 everywhere. The study was performed with isothermal walls at 293 K, a gas temperature of 313 K, and matched nominal mass flow rate/Reynolds numbers as the experiments.

Results are presented in terms of Nusselt number to remove the effect of differences in operating temperatures. The FEA results have been converted into Nusselt number, taking the average thermal conductivity of air during each test. The Nusselt number maps are presented in Figure 12 for both aspect ratio passages. The relative spatial variation in Nusselt number are in good agreement between the FEA and CFD results. However, Nusselt number is globally over-predicted. This may be attributed to error in the CFD prediction as the FEA results demonstrate close agreement to the experimental results on the planar surfaces where the experimental results can be employed without modification for surface curvature or lateral conduction.

Small differences in the structure of heat transfer are observed over the rib, particularly around the downstream edges. It is possible that this is because the mesh used in the CFD is unable to capture the more gradual changes in the heat transfer. The surface mesh used in the iterative transient FEA procedure has a spacing ~ 7.5 times greater than the one used to generate the CFD results.

Conclusion

This paper details a methodology and application of a finite element analysis method for post-processing transient TLC experimental data where one-dimensional assumptions are invalid. The method has been validated using known heat transfer coefficient distributions of high spatial gradient, and is shown to be able to provide accurate converged solutions using limited iterations of

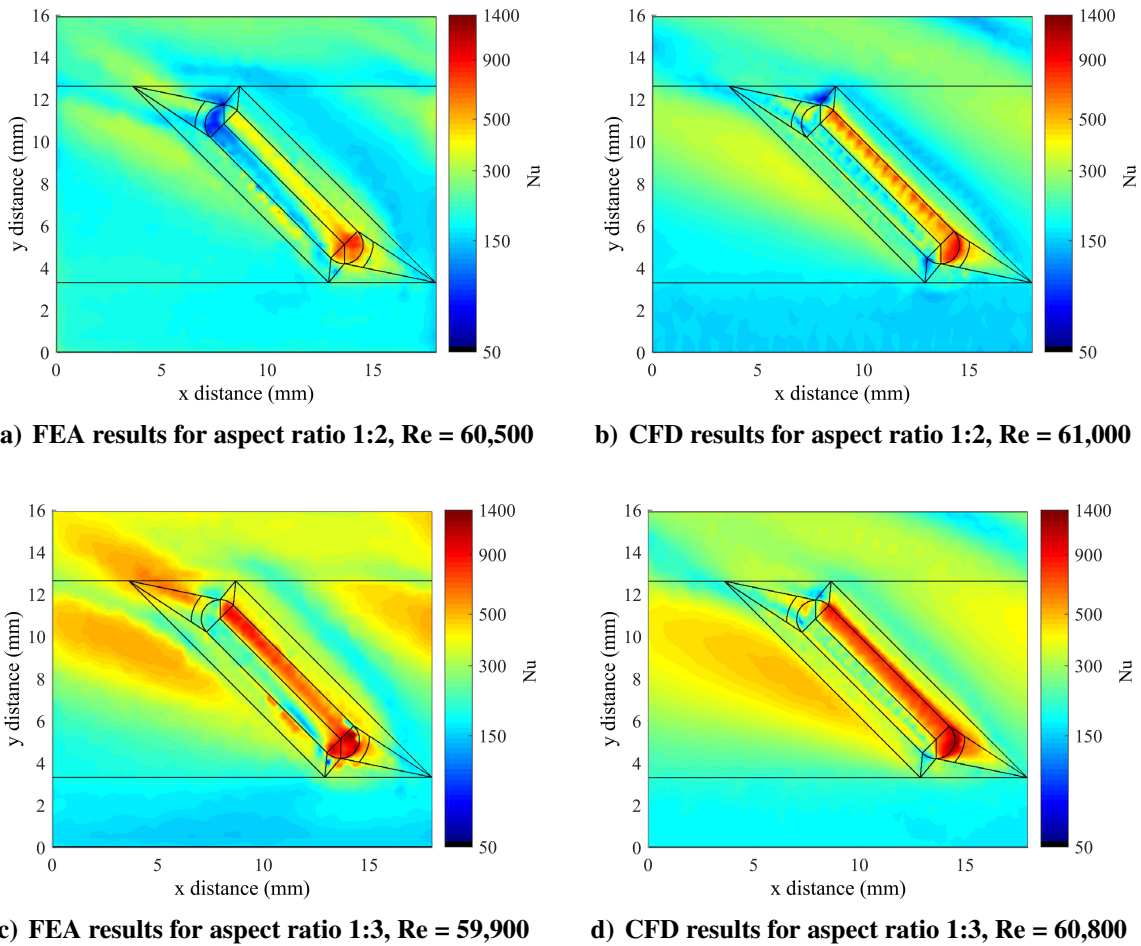


Figure 12. Nusselt number maps from Experiments and CFD

an automated algorithm.

The process has been applied to experimental data collected on an engine representative stationary model of a ribbed internal cooling passage. The analyses were conducted at five different Reynolds numbers and two aspect ratios (1:2 and 1:3). In this analysis a single rib pitch on one ribbed wall has been processed and full surface heat transfer maps produced. Agreement between the HTC derived by the FEA procedure and a purely one-dimensional approach are typically within 10% at the majority of locations on the planar surfaces. Average HTC on ribs calculated using the FEA procedure and those determined by the ‘hybrid rib’ method typically lie within 15%. Closer agreement of the average HTC values on the ribs is observed for the 1:2 aspect ratio data. Comparison of the full surface maps produced by the FEA procedure to CFD models demonstrate the same trends in Nusselt number.

Based on the validation work and the processing of the experimental data sets the transient iterative FEA method has been able to provide solutions for heat transfer under complex conditions. Improved results could be generated with data collected specifically for use of this technique with reduced noise in the intensity signals and lower heat flux. The technique developed is suitable for a wide range of heat transfer applications.

Acknowledgement

The research has received funding from the European Union Seventh Framework Programme (FP7/2007-2013) under grant agreement no. 233799 (ERICKA). Thanks also to Tony Arts at the Von Karman Institute for providing info on their FEA approach which gave us insights on beginning this work.

References

- [1] Han, J., Dutta, S., and Ekkad, S., *Gas Turbine Heat Transfer and Cooling Technology*, Taylor and Francis, 2000, ISBN: 15603284.
- [2] Coletti, F., Armellini, A., Arta, T., and Scholtes, C., “Aerothermal Investigation of a Rib-Roughened Trailing Edge Channel With Crossing Jets- Part II: Heat Transfer,” *Journal of Turbomachinery*, Vol. 133, No. 3, 2011.
- [3] Sousa, J., Lavagnoli, S., Paniagua, G., and Villafane, L., “Three-dimensional inverse heat flux evaluation based on infrared thermography,” *Quantitative InfraRed Thermography*, Vol. 9, No. 12, 2012, pp. 177–191.
- [4] Lin, M. and Wang, T., “A Transient Liquid Crystal Method using a 3-D Inverse Transient Conduction Scheme,” *International journal of heat and mass transfer*, Vol. 45, No. 17, 2002, pp. 3491–3501.
- [5] O’Dowd, D., Zang, Q., He, L., Ligrani, P., and Friedrichs, S., “Comparison of Heat Transfer Measurement Techniques on a Transonic Turbine Blade Tip,” *Journal of Turbomachinery*, Vol. 133, No. 2, 2011, pp. 21–28.
- [6] Walker, D. and Zausner, J., “RANS Evaluation of Internal Cooling Passage Geometries: Ribbed Passages and a 180 Degree Bend,” ASME Turbo Expo, Paper GT2007-278, 2007.
- [7] Hagari, T., Ishida, K., Oda, T., Douura, Y., and Kinoshita, Y., “Heat Transfer and Pressure Losses of W-shaped Small Ribs at High Reynolds Numbers for a Combustor Liner,” *Journal of Engineering for Gas Turbines and Power*, Vol. 133, No. 9, 2011.
- [8] Shevchuk, I., Jenkins, S., Weigand, B., von Wolfersdorf, J., Neumann, S., and Schnieder, M., “Validation and Analysis of Numerical Results for a Varying Aspect Ratio Two-Pass Internal Cooling Channel,” ASME Turbo Expo, Paper GT2008-51219, 2008.

- [9] Waidmann, C., Poser, R., Wolfersdorf, J. v., Foiss, M., and Semmler, K., “Investigations of Heat Transfer and Pressure Loss in an Engine Similar Two-Pass Internal Blade Cooling Configuration,” 10th European Conference on Turbomachinery, Fluid Dynamics and Thermodynamics, 2013.
- [10] Jackson, D., Ireland, P., and Cheong, B., “Combined Experimental and CFD Study of HP Blade Multi-Pass Cooling System,” ASME Turbo Expo, Paper GT2009-60070, 2009.
- [11] Ryley, J., McGilvray, M., and Gillispie, D., “Stationary Internal Cooling Passage Experiments for an Engine Realistic Configuration,” 10th European Conference on Turbomachinery, Fluid Dynamics and Thermodynamics, 2013.
- [12] Coletti, F., Facchinetti, E., and Arts, T., “Effect of Inclined Ribs on the Aero-Thermal Performance of a Trailing Edge Cavity with Crossing Jets,” 8th European Conference on Turbomachinery, Fluid Dynamics and Thermodynamics, 2009.
- [13] Forsyth, P., McGilvray, M., and Gillespie, D. R. H., “Secondary Flow and Heat Transfer Coefficient Distributions in the Developing Flow Region of Ribbed Turbine Blade Cooling Passage,” *Experimental Fluids*, Vol. 58, No. 5, 2017.
- [14] Ireland, P. T. and Jones, T. V., “Liquid crystal Measurements of Heat Transfer and Surface Shear Stress,” *Measurement Science Technology*, 2000, pp. 969–986.
- [15] Buttsworth, D. R. and Jones, T. V., “Radial Conduction Effects in Transient Heat Transfer Experiments,” *Aeronautical Journal*, Vol. 101, No. 1005, 1997, pp. 209–212.
- [16] Ling, J. P., Ireland, P. T., and Turner, L., “A Technique for Processing Transient Heat Transfer, Liquid Crystal Experiment in the Presence of Lateral Conduction,” ASME Turbo Expo, GT2003-38446, 2003.
- [17] Kingsley-Rowe, J. R., Lock, G. D., and Michael Owen, J., “Transient Heat Transfer Measurements using Thermochromic Liquid Crystal: Lateral-Conduction Error,” *International Journal of Heat and Fluid Flow*, Vol. 26, No. 2, 2005, pp. 256–263.
- [18] Brack, S., Poser, R., and Wolfersdorf, J., “An approach to consider lateral heat conduction effects in the evaluation process of transient heat transfer measurements using TLC,” *International Journal of Thermal Sciences*, Vol. 107, 2016, pp. 289–302.
- [19] Ireland, P. T., *Internal Cooling of Turbine Blades*, DPhil Thesis, University of Oxford, 1987.
- [20] Schultz, D. and Jones, T., “Heat Transfer Measurements in Short-Duration Hypersonic Test Facilities,” AGARDograph No. 165, 1973.
- [21] McGilvray, M. and Gillespie, D. R. H., “THTAC: Transient Heat Transfer Analysis Code,” Department of Engineering Science, University of Oxford, Great Britain, 2011.
- [22] Wang, Z., Ireland, P., and Jones, T., “A Technique for Measuring Convective Heat Transfer at Rough Surfaces,” *Transactions of the Institute of Measurement and Control*, Vol. 13, No. 3, 1991, pp. 145–154.
- [23] COMSOL Multiphysics, *COMSOL Version 4.2.1.110 (4.2a)*, 2010.
- [24] The MathWorks Inc., *MATLAB Version 7.10.0 (R2010a)*, 2010.
- [25] McGilvray, M., Orozco Pieiro, C., Axe, T., Ryley, J., and Gillespie, D., “Comparison of Stationary Internal Cooling Passage Experimental Data to Numerical Simulations,” 10th European Conference on Turbomachinery, Fluid Dynamics and Thermodynamics, 2013.
- [26] ANSYS Inc., *ANSYS Fluent Version 13.1*, 2012.